



Development of PLA/HA porous scaffolds with controlled pore sizes using the combined freeze drying and sucrose leaching technique for bone tissue engineering

Sunisa SINGHAWANNURAT^{1,*}, Panuwat LAWTAE¹, Catleya ROJVIRIYA², and Chalermluck PHOOVASAWAT²

¹ School of Chemical Engineering, Institute of Engineering, Suranaree University of Technology, Nakhon Ratchasima, 30000, Thailand

² Synchrotron Light Research Institute (Public Organization), Nakhon Ratchasima, 30000, Thailand

*Corresponding author e-mail: d6040253@g.sut.ac.th

Received date:

10 January 2024

Revised date:

17 March 2024

Accepted date:

12 April 2024

Keywords:

Porous scaffold;
Hydroxyapatite;
Polylactic acid;
A combined freeze drying/
sucrose leaching technique;
Porosity

Abstract

The combination of freeze drying and sucrose leaching technique was employed to fabricate PLA/HA scaffolds with controlled pore size. The influence of the HA content and sucrose size on the scaffold properties was investigated. The fabricated scaffolds showed porous properties with a porosity of 44% to 58% and pore size of 461 μm to 688 μm . The results indicated that the scaffolds possessed favorable porous properties, illustrated by good interconnectivity, appropriate pore size, and suitable porosity. These characteristics were crucial for facilitating bone cell growth and promoting the formation of new tissue within the scaffold structure. The compressive modulus of the scaffolds was examined and found to be in the range of 3.35 MPa to 5.75 MPa. Furthermore, the degradation behavior of the scaffolds was studied for 28 days in a Phosphate Buffered Saline solution. The results showed that the degradation rate was varied in the range of 6% to 14%. The water uptake of the scaffolds exhibited a range between 180% and 200%. Enhancement in water uptake was observed with higher HA content and increased sucrose size. Consequently, the scaffolds developed in this study hold promise as optimal candidates for bone tissue engineering applications.

1. Introduction

Bone loss can occur from various conditions, such as traumatic accidents, cancer, fractures, osteoporosis, and congenital pseudarthrosis [1]. Surgical grafting techniques, such as autograft, allograft, and xenograft, have been employed to address bone tissue loss [2,3]. However, these techniques have limitations, which are the requirement for donor sites and the risk of immunological rejection [4]. As a result, innovative approaches are being sought, and bone tissue engineering has emerged as a promising solution [5]. This approach involves the use of scaffolds to support seeded cells and facilitate the development of desired tissue. Bone tissue engineering offers customization and patient-specificity for bone regeneration [6].

An ideal scaffold for bone tissue engineering should possess non-toxicity, good biocompatibility, biodegradability, high porosity, and optimal mechanical properties [7,8]. Hydroxyapatite (HA), a fundamental component of human bone, has been extensively used in bone tissue engineering due to its biocompatibility, bioresorbability, and osteo-conductivity [9]. However, the weak fracture toughness and brittle characteristics of HA restrict its utility in load-bearing applications [10]. To overcome these limitations, researchers have investigated composite scaffolds combining HA with polymers, such as polylactic acid (PLA), polyglycolic acid (PGA), and their copolymers (PLGA), due to their biocompatibility, biodegradability, and tunable mechanical properties [11]. PLA, in particular, has been extensively studied in bone tissue engineering due to its beneficial

characteristics, including non-toxicity, processability in various forms, favorable mechanical properties, and controllable degradation for the gradual release of drugs or growth factors [12,13].

Fabrication techniques of scaffolds are a critical factor influencing the properties and performance of the resulting scaffold. Scaffold fabrication techniques can be broadly categorized into two categories: conventional and advanced techniques [14]. While advanced techniques like electrospinning [15] and 3D printing [16] have gained significant attention in recent years, conventional techniques such as salt leaching [17], melt molding [18], gas foaming [19], phase separation [20], and freeze drying [21] remain popular due to their simplicity and ability to create highly porous and interconnected scaffolds. However, achieving precise control over pore size and interconnected porosity in conventional techniques poses a significant challenge. One commonly employed method for achieving desired pore sizes is salt leaching, but it is accompanied by limitations, such as the dissolution and fracturing of the porogen during mixing and molding, resulting in variations in scaffold pore size [22,23]. To address these challenges, a combination of conventional techniques has been explored, particularly the combination of salt leaching and freeze drying [24]. Freeze drying is well-known for its effective preservation of scaffold structures during fabrication [25]. By incorporating freeze drying with salt leaching, better control over pore size, interconnected porosity, and scaffold structure maintenance can be achieved [12]. Additionally, the choice of porogen material significantly influences the pore structure of the scaffold. Dorati *et al.* [26] investigated the effect of different porogens

(salt and sugar) on scaffold properties and found that scaffolds fabricated using salt particles exhibited a more irregular pore structure compared to those using sucrose crystals as porogens. It is likely due to the dissolution and fracturing of the salt particles during the mixing and molding process. This led to variations in pore size and shape within the scaffold. In contrast, sucrose crystals, with their regular shape and higher solubility, allowed for controlled leaching, resulting in more consistent and organized pore structures. Thus, sucrose is selected as the porogen in this work to ensure the formation of scaffolds with uniform and well-defined pore structures.

This study presents a modified method for fabricating PLA/HA porous scaffolds with controlled pore sizes using a combination of freeze drying and sucrose-leaching techniques. The investigation focuses on the influence of HA content and sucrose size on various properties of the porous scaffold, including porosity, surface area, density, and equivalent pore diameter, as well as the chemical structure, surface functional groups, and surface morphology. Moreover, mechanical strength testing, degradation, and water uptake analysis are conducted to evaluate the performance of the scaffolds. The findings of this study provide valuable insights into the development of scaffolds with precise control over pore sizes tailored to meet the specific requirements for diverse biomedical applications, especially in the field of bone tissue engineering

2. Material and experimental

2.1 Materials

Biopolymer PLA 2003D ($M_w = 120,000 \text{ g}\cdot\text{mol}^{-1}$) was purchased from NatureWorks (USA). Hydroxyapatite nanoparticle (HA, 99%) with a particle size of 60 nm was obtained from Chanjao Longevity Co., Ltd. (Thailand). 1,4-dioxane (99%) purchased from Carlo Erba (Italy) was used as a solvent for PLA. Sucrose was supplied from a convenience store. The sucrose was sieved to obtain a sucrose size of 250 μm to 850 μm .

2.2 Porous scaffold fabrication

The combined freeze drying and sucrose leaching technique was utilized to fabricate the porous scaffold with the desired pore size range. The PLA/HA scaffolds were prepared using the following procedure:

First, 10 g of PLA was dissolved in 1,4-dioxane, which served as the solvent, to obtain a 10% w/v PLA solution. The solution was stirred at a constant temperature of 70°C until a homogeneous solution was obtained. HA particles were then added to the PLA solution and further

stirred for 1 h at 70°C to ensure complete dispersion within the solution. Sucrose particles, used as the porogen, were added with continuous stirring for 10 min to achieve uniform dispersion and prevent sucrose breakage. The resulting slurry mixture was poured into PTFE molds with a diameter of 10 mm.

Next, the scaffold samples were placed in a freezer and kept at -60°C for 24 h. Subsequently, the frozen samples were dried at -70°C and at a pressure of 0.110 mbar for 24 h in a freeze dryer to completely remove the solvent. The samples were carefully removed from the molds and cut to obtain cylindrical scaffolds with a diameter of 10 mm and a length of 12 mm. Finally, the porous scaffolds were obtained through sucrose leaching by soaking them in deionized water for 48 h, followed by drying with air at 60°C for 24 h.

The HA content in the range of 10% to 20% and various sucrose size ranges were investigated. The sucrose content in the slurry was maintained at a ratio of 0.9 g of sucrose per gram of slurry to ensure its uniform distribution within the scaffold structure. The porous scaffold samples were designated as SCx-y, where SC stands for scaffold, the symbol x represents the sucrose lower-size range, and y represents the percentage of HA. Table 1 summarizes the preparation parameters for fabricating the porous scaffolds.

2.3 Characterization of the fabricated scaffolds

2.3.1 Porous properties

The porous properties of the scaffolds were examined using synchrotron radiation X-ray tomographic microscopy (SRXTM) at the X-ray Imaging and X-ray Tomographic Microscopy Beamline (BL1.2W) located at the Synchrotron Light Research Institute (SLRI) in Nakhon Ratchasima, Thailand. Sample projections were acquired using a detection system with a scan angle ranging from 0° to 180° and an angular increment of 0.1° . The tomographic data were collected with a pixel size of 3.61 μm . Subsequently, the data were normalized using the flat-field correction algorithm and reconstructed using Octopus reconstruction. The specific surface area and porosity were determined through Octopus analysis. The equivalent pore diameter was calculated by Image J. Three-dimensional images were generated using Drishti software. Additionally, the bulk density (ρ) of the scaffolds was calculated using the following Equation (1).

$$\rho = \frac{W}{\pi \times (D/2)^2 \times h} \quad (1)$$

Where ρ represents the scaffold density ($\text{g}\cdot\text{cm}^{-3}$), W is the weight, D is the diameter, and h is the thickness of the dried scaffolds.

Table 1. Preparation parameters for fabricating the porous scaffolds.

Sample name	Sucrose content ($\text{g}\cdot\text{g}^{-1}$)	Sucrose size range (μm)	HA content (wt%)
SC250-10	0.9	250 to 425	10
SC425-10	0.9	425 to 600	10
SC425-15	0.9	425 to 600	15
SC425-20	0.9	425 to 600	20
SC600-10	0.9	600 to 850	10

2.3.2 Chemical structure and morphological analysis

The chemical structure and functional groups present in the scaffolds were analyzed using Fourier Transform Infrared (FT-IR) spectroscopy (TENSOR 27-Hyperion, BRUKER). The FTIR spectra were obtained in the wavenumber range of 400 cm⁻¹ to 4000 cm⁻¹ with a measurement resolution of 4 cm⁻¹. The elemental composition of the scaffold surfaces was examined using Energy Dispersive X-ray Fluorescence (XGT-5200, HORIBA). The analysis was performed at an X-ray tube voltage of 30 kV, and the irradiation spectrum was acquired for 100 s. Furthermore, the microstructure and surface morphology of the scaffolds were observed using a Scanning Electron Microscope (JEOL/JSM-6010LV model, HITACHI). Before imaging, the samples were appropriately sized and coated with a thin layer of gold (Au).

2.3.3 Mechanical testing

The mechanical properties of the scaffolds were evaluated using an electronic universal testing machine to measure the compressive modulus. The cylindrical scaffolds were subjected to compression along their axial direction at room temperature. A compressive load was applied to achieve a total strain of 80% at a constant compression speed of 1 mm·min⁻¹. The compression test was conducted three times, and the average value was reported. The compressive modulus (E) was determined by calculating the slope of the initial linear portion of the stress-strain curve using the following Equation (2).

$$E = \frac{\sigma}{\epsilon} \quad (2)$$

Where E represents the compressive modulus (MPa), σ is the applied compressive stress (MPa), and ϵ denotes the compressive strain (mm·mm⁻¹).

2.3.4 Degradation analysis

The cylindrical scaffolds were subjected to in vitro degradability analysis by immersing them in a Phosphate Buffered Saline (PBS) solution. A total of 20 mL of PBS solution with a pH of 7.4 was placed in a Duran bottle, and the scaffolds were immersed in the solution. The degradability study was conducted at 37°C for different time intervals of 1, 3, 7, 14, 21, and 28 days. The weight of the dried scaffolds was measured before and after immersion in PBS to determine the degradation percentage using the following Equation (3).

$$\% \text{ Degradation} = \frac{W1 - W2}{W1} \times 100 \quad (3)$$

Where W1 represents the initial dry weight of the scaffolds, and W2 represents the dry weight of the scaffolds after removal from the PBS solution for a specific time duration.

2.3.5 Water uptake capacity

The water uptake of the scaffolds was evaluated using a gravimetric method. The cylindrical specimens were submerged in 10 mL of deionized water for 24 h. Following immersion, the scaffolds were carefully extracted and subjected to a blotting procedure using filter paper to remove excess surface water. The water uptake was then calculated using the following Equation (4).

$$\text{Water uptake} = \frac{W_{\text{wet}} - W_{\text{dry}}}{W_{\text{dry}}} \times 100 \quad (4)$$

Where W_{wet} and W_{dry} represent the weights of the water-saturated and dry scaffold specimens, respectively.

3. Results and discussion

3.1 Porous properties of the fabricated scaffolds

Figure 1 showed the 3D structure and internal constitution of the fabricated scaffolds, prepared using the combined freeze drying and sucrose leaching technique. The influence of sucrose size on the pore structure of the fabricated scaffolds could be observed in Figure 1(a-c). The results clearly demonstrated that the pore structure of the scaffolds was directly influenced by the chosen sucrose size. In addition, Figure 1 also showed the uniform dispersion of the sucrose in the PLA/HA solution during the preparation of the porous scaffolds. The effect of sucrose size on the porous properties of the fabricated scaffolds was summarized in Table 2. The samples, namely SC250-10, SC425-10, and SC600-10, corresponded to scaffold porosities of 44%, 52%, and 58%, respectively. Based on the lower sieve size range of the employed sucrose, the relationship between sucrose size and scaffold porosity demonstrated a nearly linear trend, with an approximate increase of 0.04% per μm , as depicted in Figure 2. These findings revealed a significant increase in scaffold porosity with an increase in sucrose size. Moreover, as the porosity increased, the specific surface area tended to decrease from 3.24 cm²·g⁻¹ to 1.93 cm²·g⁻¹ (see Figure 2). This could occur due to larger pores occupying a greater volume within the material, resulting in a diminished surface area available per unit mass. These observations aligned with the typical porous properties observed in porous materials, where larger pore sizes lead to reduced surface area and material density.

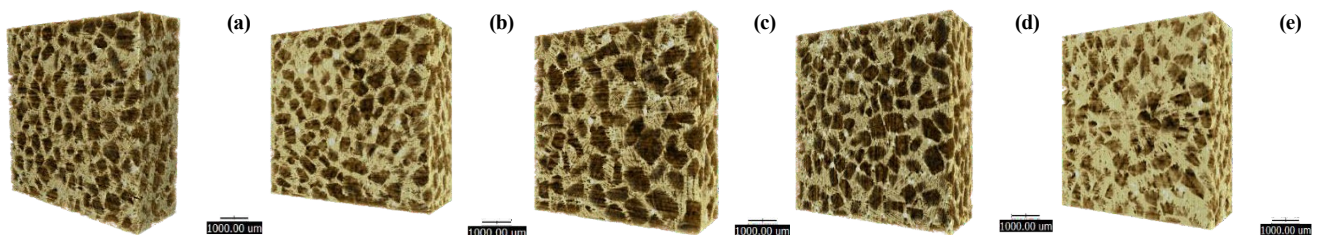
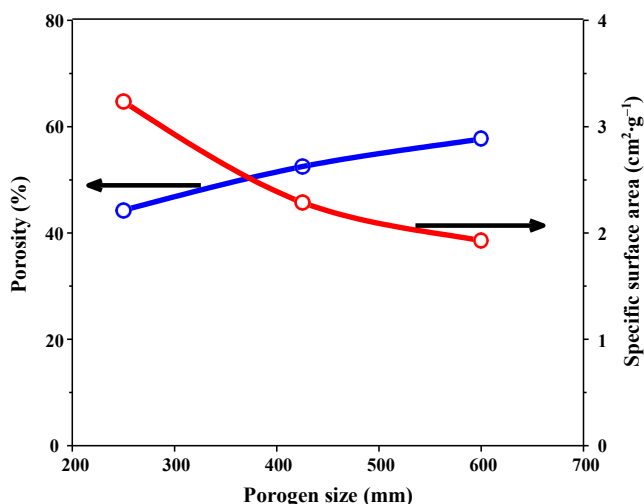


Figure 1. Three-dimensional structure and internal constitution of the fabricated scaffolds: (a) SC250-10, (b) SC425-10, (c) SC600-10, (d) SC425-15, and (e) SC425-20, as observed through Synchrotron radiation X-ray tomography.

Table 2. Porous properties and densities of the fabricated scaffolds.

Sample name	Equivalent diameter (μm)	Porosity (%)	Specific surface area ($\text{cm}^2\text{-g}^{-1}$)	Density ($\text{g}\cdot\text{cm}^{-3}$)
Sucrose size				
SC250-10	480.57 ± 151.81	44.29	3.237	0.160 ± 0.008
SC425-10	485.83 ± 100.29	52.50	2.288	0.152 ± 0.008
SC600-10	687.54 ± 183.69	57.68	1.930	0.141 ± 0.003
HA content				
SC425-10	485.83 ± 100.29	52.50	2.288	0.152 ± 0.008
SC425-15	449.20 ± 169.71	48.85	2.343	0.165 ± 0.007
SC425-20	461.34 ± 151.81	40.81	2.728	0.197 ± 0.004

**Figure 2.** Influence of Sucrose size on the porosity and specific surface area of the porous scaffolds.

Regarding the equivalent pore diameter, it was noteworthy that all fabricated scaffolds, except for the SC250-10 sample, fell within the sucrose size ranges. The SC250-10 sample exhibited a larger equivalent pore diameter than the upper size range (250 μm to 425 μm) by approximately 13%. This could be attributed to the agglomeration of the sucrose during the preparation process, which was likely influenced by the stirring rate. However, increasing the stirring rate might result in sucrose breakage, leading to smaller pore sizes within the scaffolds. It was important to note that the suitable pore size range for bone growth scaffolds typically ranges from 300 μm to 1000 μm [27]. This range played a crucial role in providing structural guidance to cells, facilitating nutrient transport, promoting tissue regeneration, and enabling efficient cell infiltration. Therefore, the fabricated scaffolds in this study offered a suitable pore size range for use as bone-porous scaffolds.

The effect of HA content on the fabricated scaffolds was also investigated. As shown in Table 2, increasing the HA content from 10% to 20% resulted in a corresponding increase in the density of the scaffolds by approximately 30%, ranging from 0.15 $\text{g}\cdot\text{cm}^{-3}$ to 0.20 $\text{g}\cdot\text{cm}^{-3}$. The results indicated that a higher percentage of HA content contributes to the formation of a denser structure in the porous scaffolds as shown in Figure 1(b), Figure 1(d), and Figure 1(e), enhancing their mechanical strength. A slight increase in specific surface area was also observed as the HA content increased. This was likely involved in the size of the pore formation that occurred during solvent removal. It was important to note that the pore collapse during

solvent removal might occur because of the less dense nature of the scaffolds. When the HA content was increased, resulting in a denser structure, hence the surface area was possibly higher compared to that of the fabricated scaffolds using lower levels of HA content. On the other hand, the porosity of the scaffolds decreases by about 7% and 16.5% for an increase in the HA content to 15% and 20%, respectively. This decrease in porosity could be attributed to the decrease in solvent volume caused by increasing HA concentration, resulting in fewer pores formed by solvent sublimation during freeze drying. It should be noted that the porosity of bone tissue can generally be classified into cortical bone (dense bone) with a porosity range of 5% to 15% and trabecular bone (spongy bone) with a porosity range of 40% to 95% [28]. Therefore, the fabricated scaffolds in this study fell within the porosity range of trabecular bone, indicating the suitability of the achieved porosity in this work.

3.2 Chemical structure analysis of the fabricated scaffolds

FTIR spectroscopy was employed to analyze the chemical structure of the PLA/HA scaffolds prepared using the combined freeze drying and sucrose leaching technique, as shown in Figure 3. The FTIR spectra of hydroxyapatite (HA) exhibited characteristic peaks at approximately 561 cm^{-1} , 601 cm^{-1} , and 1024 cm^{-1} , attributed to the stretching vibration bands of the phosphate group (PO_4^{3-}) [29,30]. The FTIR spectra of the fabricated scaffolds displayed patterns similar to those of HA, confirming the presence of HA within the scaffolds. Furthermore, additional peaks observed at approximately 1087 cm^{-1} and 1183 cm^{-1} corresponded to the C–O stretching in esters, and a small peak ranging from 1360 cm^{-1} to 1384 cm^{-1} suggested the presence of methyl group bending modes [31,32]. A sharp peak at 1755 cm^{-1} indicated the stretching vibration of the carbonyl group (C=O) [33]. These peaks, consistent with pure PLA spectra [34], provided evidence for the coexistence of HA and PLA in the PLA/HA scaffolds.

To examine the HA composition in the fabricated scaffolds, the Ca/P ratio was determined using Energy Dispersive X-ray Fluorescence (ED-XRF). Figure 4 illustrated the relationship between the Ca/P ratio and the percentage of HA content in the scaffolds, comparing the results from this study with those of previous investigations. The results revealed that the Ca/P ratio of the PLA/HA scaffolds ranged from 1.63 to 1.89 (Table 3), which fell within the range reported in previous studies (1.33 to 2.48) [10,12,35-38]. These variations in the Ca/P ratio of composite scaffolds could arise from differences in fabrication methods and HA compositions. It was noteworthy that although the ideal Ca/P ratio for hydroxyapatite was commonly considered as

1.67, deviations had been reported in the literature for both synthesized and commercial HA samples. For instance, Chaikina *et al.* [39] reported a Ca/P ratio ranging from 1.5 to 1.9 for synthesized HA. Similarly, Mohd *et al.* [40] synthesized HA with a Ca/P ratio in the range of 1.5 to 2. Best *et al.* [41] investigated two different commercial HA samples, finding Ca/P ratios of 1.65 and 1.76, respectively. Overall, the Ca/P ratio of the PLA/HA scaffolds in this study was consistent with the reported values in the literature, supporting the composition of HA within the scaffolds.

3.3 Microstructure and morphology of the fabricated scaffolds

Figure 5 showed the microstructure and surface morphology of the fabricated scaffolds obtained from SEM images. Figure 5(a-c) presented the fabricated scaffolds using various sucrose sizes with the lower-sieve size range of 250 μm , 425 μm , and 600 μm , respectively. The SEM images provided evidence of a discernible trend between the employed sucrose size and the resulting equivalent pore diameter, although the observed change was not very pronounced. These results were consistent with the findings regarding the equivalent pore diameter and porosity presented in Table 2.

It was worth noting that the scaffolds exhibited a distribution of small pores throughout their structure, which was attributed to the sublimation of the solvent (1, 4-dioxane) during the freeze drying process. The equivalent pore diameter of these pores was measured to be approximately 12 μm to 17 μm using ImageJ software. These pores play a crucial role in promoting interconnectivity between the larger pores, facilitating the transport of nutrients and waste within the scaffolds. The choice of 1, 4-dioxane as the solvent for PLA dissolution was based on its low melting point, liposolubility, and highly volatile nature. Previous studies by Aboudzadeh *et al.* [42] compared the use of two different solvents, namely 1,4-dioxane, and N-methyl-2-pyrrolidone, for PLA dissolution in scaffold fabrication. It was found that scaffolds fabricated with 1,4-dioxane exhibited higher rates of porosity, interconnectivity, bioactivity, and biocompatibility, mainly due to the solvent's higher evaporation rate when compared to N-methyl-2-pyrrolidone. In addition to the properties of the raw materials used, factors related to the freeze drying process, such as condenser temperature, chamber pressure, and freeze drying time, could also influence the porous properties of the scaffolds [43]. However, in the development of porous scaffolds, it was imperative to carefully consider the balance between their porous properties and mechanical

characteristics to ensure their optimal efficacy as bone tissue scaffolds. Thus, the mechanical characteristic of the fabricated scaffolds was presented and discussed in the following section.

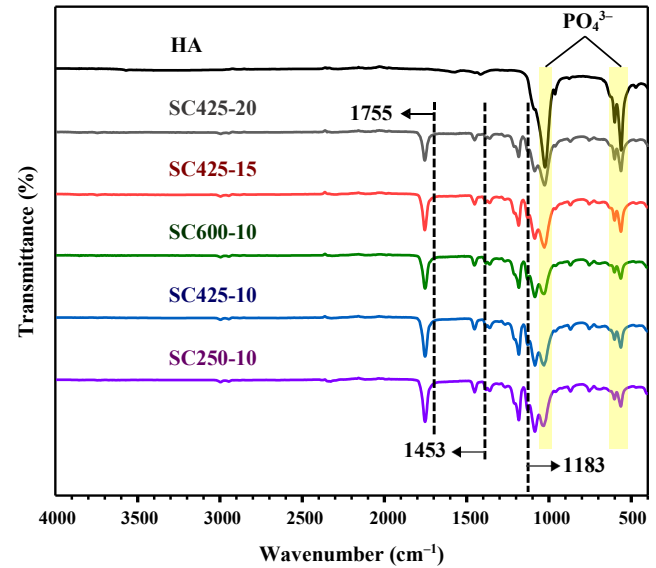


Figure 3. The FTIR spectra of hydroxyapatite (HA) and the PLA/HA scaffolds were fabricated using the combined freeze drying and sucrose leaching technique.

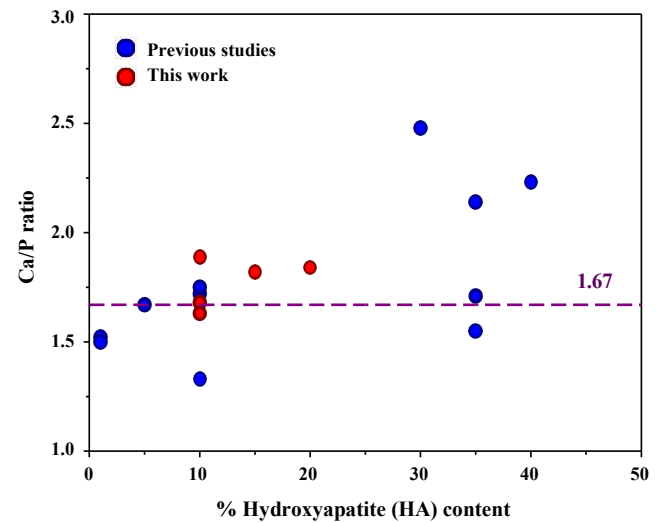


Figure 4. Comparison of the Ca/P ratio of the scaffolds with various percentages of hydroxyapatite used from the present study and previous studies [10,12,35-38].

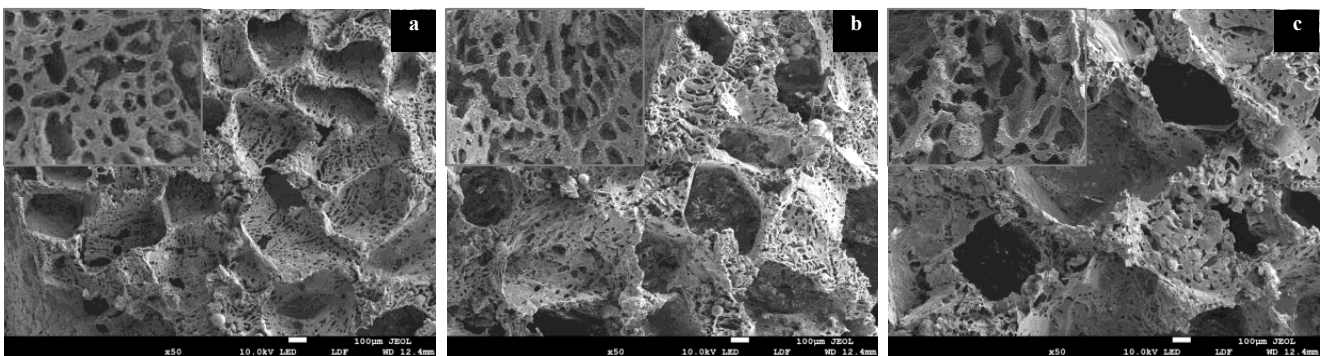


Figure 5. SEM image of (a) SC250-10, (b) SC425-10, and (c) SC600-10.

3.4 Mechanical properties of the scaffolds

The compression test was performed on the PLA/HA scaffolds. The stress-strain curve exhibited three distinct stages as shown in Figure 6(b). The first stage displayed a linear elastic region, indicative of proportional loading. This was followed by a plateau stage characterized by a relatively constant stress level despite increasing strain. This behavior suggested a stress accommodation mechanism, potentially due to pore collapse or microcrack formation within the scaffold structure. The final stage manifested as an exponential rise in stress, signifying the densification of the material. The compressive modulus of the fabricated scaffolds was determined and illustrated in Figure 6(a). The modulus, which represented the elastic characteristics of the scaffolds, was determined from the slope of the linear region of the stress-strain curve. The results indicated that the compressive modulus increased from 3.65 MPa to 3.78 MPa when the HA content was increased from 10% to 20%. This emphasizes the significant reinforcing effect of hydroxyapatite (HA) on the elastic properties of the scaffold matrix. As expected, the PLA/HA scaffolds with a higher HA ratio exhibited a higher compressive modulus due to the substantial stiffness of HA as a ceramic material, with an elastic modulus of approximately 35 GPa [44]. These results were consistent with previous studies by Hassanajili *et al.* [12], who investigated the effect of HA content ranging from 30% to 50% on the compressive modulus of the scaffolds.

Their findings revealed an increase in the compressive modulus from 0.5 MPa to 1.1 MPa, further supporting the significant reinforcing effect of HA on the elastic properties of the scaffold matrix.

The SC250-10 scaffold, composed of 10% HA and a sucrose size range of 250 μm to 425 μm , exhibited a remarkable maximum compressive modulus of approximately 5.75 MPa. This value was notably higher than the average compressive modulus of all samples by approximately 42%, whereas the scaffold with the largest sucrose size (SC600-10) had a compressive modulus lower than the average by about 18%. These findings strongly suggested a notable influence of sucrose size on the compressive modulus. This influence could be attributed to two primary factors. Firstly, an increase in sucrose size led to a higher overall porosity, which generally correlates with a decrease in compressive modulus. This finding was consistent with previous studies investigating the effect of porosity on the compressive modulus, as reported by Conrad *et al.* and Cho *et al.* [22,23]. Secondly, an increase in sucrose size could result in a potentially varied proportion of the Ca/P ratio within the scaffolds, which led to a variation of pure hydroxyapatite, hence giving a lower compressive modulus. This notion was further supported by the fact that the SC250-10 scaffold has a Ca/P ratio (1.68) closest to the ideal Ca/P ratio for hydroxyapatite (1.67) (see Table 3). Therefore, the higher compressive modulus observed in the SC250-10 scaffold, compared to other samples, could be attributed primarily to the presence of pure hydroxyapatite within the scaffolds.

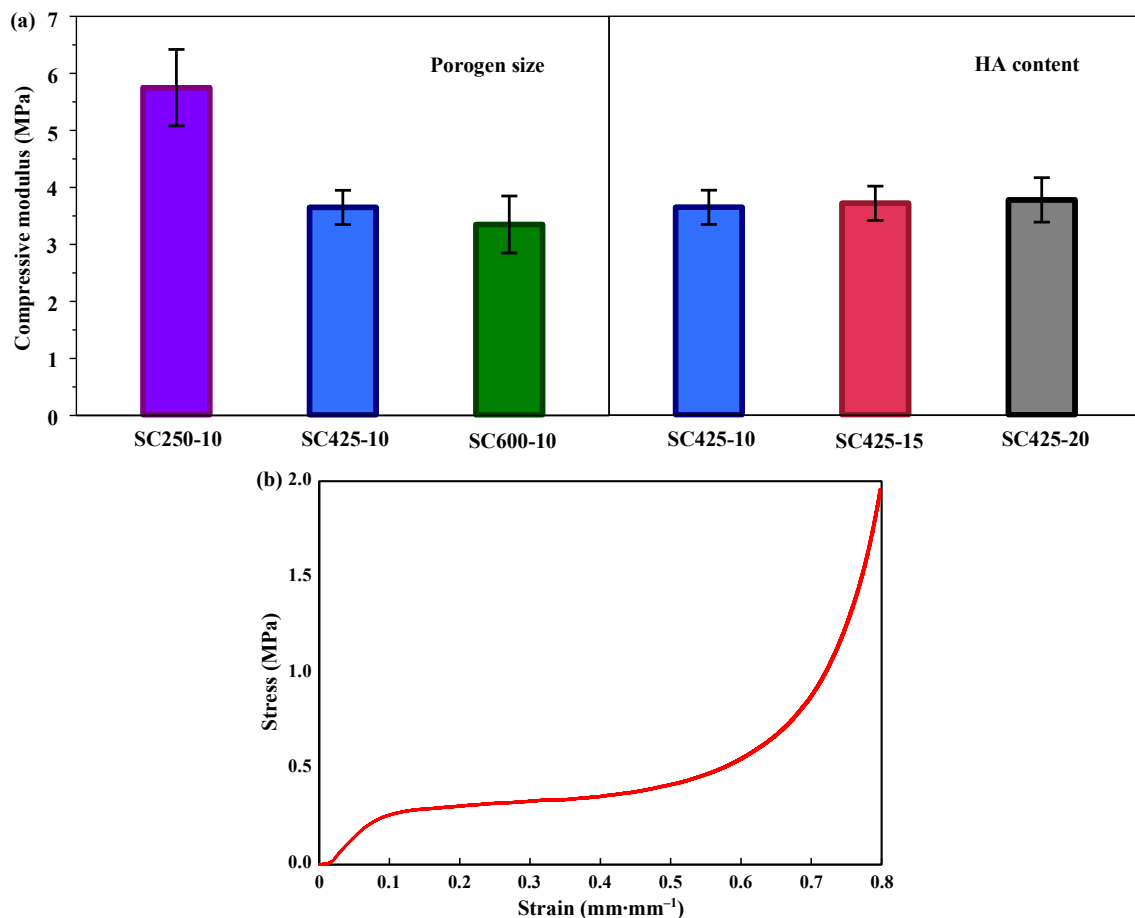


Figure 6. (a) Effect of sucrose size and hydroxyapatite content on the compressive modulus of the porous scaffolds prepared in this study (b) the stress-strain curve of the scaffold.

Furthermore, it was worth noting that porous scaffolds fabricated using the freeze drying technique generally exhibit a low compressive modulus, as indicated in Table 4. For example, Huang *et al.* [45] developed gelatin/bioactive glass composite scaffolds using a combination of casting and freeze-drying, resulting in a compressive modulus of 56 kPa to 60 kPa after immersion in simulated body fluid (SBF). Similarly, Li *et al.* [38] prepared chitosan-hydroxyapatite composite scaffolds using freeze drying and cold atmospheric plasma technology, with a modulus ranging from approximately 0.5 MPa to 1.2 MPa. In comparison, the scaffolds fabricated in this study demonstrated a higher compressive modulus than the aforementioned studies. However, it was essential to maintain a balance between achieving an appropriate porosity range of 40% to 95% [28] to facilitate cell infiltration and nutrient transport and ensuring sufficient mechanical properties to support cell growth and maintain scaffold integrity, specifically, the compressive modulus of bone scaffolds should be in the range of 2 MPa to 10 MPa [46].

3.5 Degradability of the scaffolds

The degradation behavior of the fabricated scaffolds was performed and measured by the percentage of mass loss during a 28 day immersion in a PBS solution, as illustrated in Figure 7. It was observed that scaffolds with a higher HA content exhibited a lower percentage of degradation. This could be attributed to the inherent properties of HA, which a ceramic material was known for

its higher resistance to degradation compared to the polymer matrix. The presence of a higher proportion of HA in the scaffold composition, therefore, contributed to its enhanced degradation resistance. Furthermore, an increase in sucrose size, particularly observed in SC600-10, resulted in a significantly slower rate of degradation compared to other samples. This was likely due to the decrease in the surface area of the scaffold caused by larger pores, hence giving a lower diffusion flux of PBS within the pores. As a result, SC600-10 exhibited a relatively low degradation rate.

Consideration of the long term degradation characteristics of bone scaffolds was crucial for assessing their potential clinical applications and biocompatibility. The degradation period of bone scaffolds should depend on the application requirements such as scaffolds utilized in spinal fusion applications (9 month or longer), and scaffolds employed in cranio-maxillofacial applications (3 month to 6 month) [49]. This study focused on the short term degradation behavior over 28 days in PBS and the observed percentage of degradation rate for all scaffolds ranged from approximately 6% to 14%. It could be inferred that the degradation period of the fabricated scaffolds would be in the range of 7 month to 15 month in the PBS solution. Therefore, it could be said that the scaffolds prepared in this work have the potential for use in bone applications. However, the degradation in the body's physiological environment might occur faster degradation rate due to the presence of enzymes and other biological factors that can influence the degradation process.

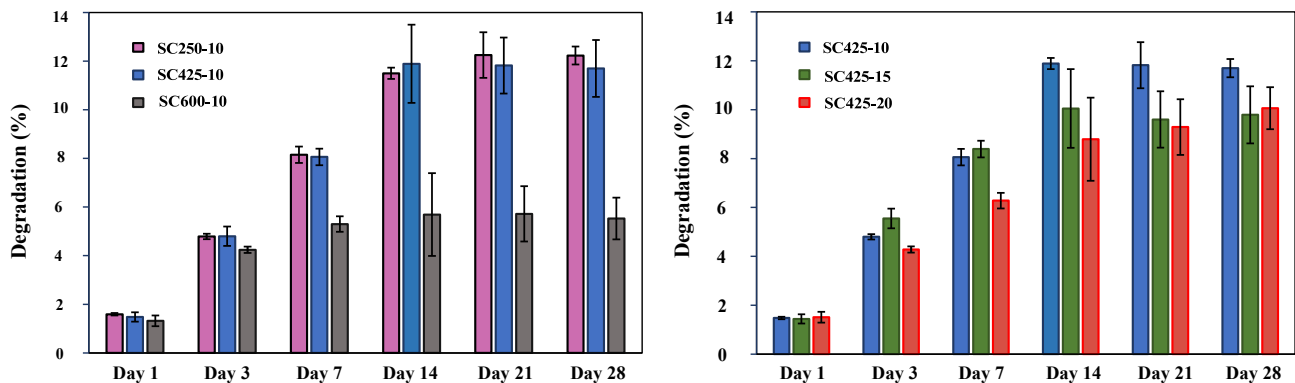


Figure 7. Effect of hydroxyapatite content (left) and sucrose size (right) on the degradability of the porous scaffolds over 28 days.

Table 3. Ca/P ratio of the fabricated scaffolds.

Sample name	Ca/P ratio
SC250-10	1.68 ± 0.02
SC425-10	1.89 ± 0.04
SC600-10	1.63 ± 0.03
SC425-15	1.89 ± 0.04
SC425-20	1.84 ± 0.05

Table 4. The compressive modulus of porous scaffolds fabricated using the combination of freeze-drying with various techniques.

Precursor	Fabrication technique	Compressive modulus (MPa)	Ref.
Gelatin/phosphate glass	Freeze drying	1.02 to 4.89	[21]
zein/chitosan/HA	Freeze drying	3.8 to 7.5	[47]
PLA/PCL/HA	Freeze drying with Indirect 3D printing	0.5 to 1.35	[12]
Chitosan/agarose/HA	Foaming agent with freeze drying	11.79 to 13.98	[48]
Chitosan/HA	Freeze drying and cold atmospheric plasma technology	0.6 to 1.14	[38]
PLA/HA	Freeze drying and porogen leaching	3.65 to 5.75	This work

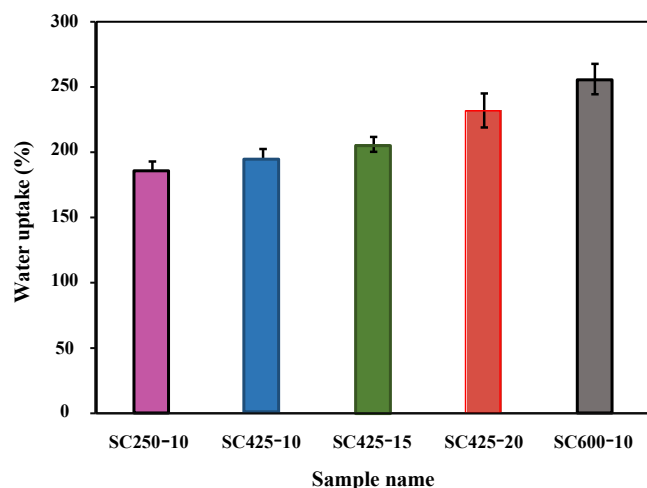


Figure 8. Effect of hydroxyapatite content and sucrose size on the water uptake of the porous scaffolds over 24 h.

3.6 Water uptake of the scaffolds

Scaffolds with high water content were proposed to recapitulate key features of the natural extracellular matrix, potentially influencing cell migration, proliferation, and organization during tissue repair and regeneration. This biomimetic approach holds particular promise for tissues characterized by inherent hydrophilicity, such as cartilage, cornea, liver, nervous tissue, and bone, where scaffolds with high water uptake may exhibit superior compatibility.

The water uptake of PLA/HA scaffolds was shown in Figure 8. Scaffolds with a higher HA content displayed a significant increase in water uptake. This phenomenon could be attributed to the inherent hydrophilicity of HA molecules. The hydroxyl groups presented along the HA form strong hydrogen bonds with water molecules, promoting their adsorption within the scaffold structure. Consequently, a higher proportion of HA in the scaffold composition directly translated to an enhanced capacity for water uptake.

4. Conclusions

In this study, the PLA/HA porous scaffolds were successfully fabricated using the combination of freeze drying and sucrose leaching techniques, allowing for precise control of pore size. The pore structure of the scaffolds was directly influenced by the size of the sucrose. The pore size of the scaffolds aligned with the size of the sucrose employed, except for the SC250-10 sample, which could be attributed to the agglomeration of sugar during the preparation process. The increase in HA content contributed to the enhancement of the compressive modulus in the scaffolds. Among all the samples, it was observed that the SC250-10 sample, which consisted of a composition of 10% hydroxyapatite and utilized sucrose with a size range of 250 μm to 425 μm , exhibited the highest compressive modulus. It could be explained by the appropriateness of both the sucrose size proportion and the PLA/HA composition within the scaffold. Furthermore, the Ca/P of SC250-10 (1.68) closely approximated the Ca/P of ideal hydroxyapatite (1.67). The degradation behavior of the fabricated scaffolds was evaluated through a 28 day immersion in a PBS solution. The structure of the scaffolds with a higher proportion of

hydroxyapatite contributed to its enhanced degradation resistance. The SC600-10 sample, which had a sucrose size range of 600 μm to 800 μm , exhibited the minimum degradation rate caused by the decrease in the surface area of the scaffold. The water uptake of the scaffolds was determined by immersed in deionised water for 24 h. The results revealed that the HA content could improve the hydrophilic of the scaffold with up-regulated water uptake capacity. Additionally, when sucrose size was increased, there was a significant increase in water uptake due to larger pores and higher porosity in the scaffold creating more space for water adsorption. It believed that the fabricated scaffold in this study had suitable properties and potential to be used as the scaffold for bone tissue engineering.

Acknowledgements

The authors gratefully acknowledge the support in the form of graduate scholarship to Sunisa Singhawannurat from Suranaree University of Technology (SUT). The authors also would like to thank the Center for Scientific and Technological Equipment, SUT for supporting the analytical instruments used in this work.

References

- [1] R. Dimitriou, E. Jones, D. McGonagle, and P. V. Giannoudis, "Bone regeneration: current concepts and future directions," *BMC Medicine*, vol. 9, no. 1, p. 66, 2011.
- [2] C. Kieman, C. Knuth, and E. Farrell, "Chapter 6 - endochondral ossification: recapitulating bone development for bone defect repair," in *Developmental Biology and Musculoskeletal Tissue Engineering*, M. J. Stoddart, A. M. Craft, G. Pattappa, and O. F. W. Gardner Eds. Boston: Academic Press, pp. 125-148, 2018.
- [3] A. Ibrahim, "13 - 3D bioprinting bone," in *3D Bioprinting for Reconstructive Surgery*, D. J. Thomas, Z. M. Jessop, and I. S. Whitaker Eds.: Woodhead Publishing, pp. 245-275, 2018.
- [4] M. S. Carvalho, J. Cabral, C. Silva, and D. Vashishth, "Bone matrix non-collagenous proteins in tissue engineering: creating new bone by mimicking the extracellular matrix," *Polymers*, vol. 13, p. 1095, 2021.
- [5] S. Pramanik, S. Kharche, N. More, D. Ranglani, G. Singh, and G. Kapusetti, "Natural biopolymers for bone tissue engineering: A brief review," *Engineered Regeneration*, vol. 4, no. 2, pp. 193-204, 2023.
- [6] B. N. Kharbikar, J. X. Zhong, D. L. Cuylear, C. A. Perez, and T. A. Desai, "Theranostic biomaterials for tissue engineering," *Current Opinion in Biomedical Engineering*, vol. 19, p. 100299, 2021.
- [7] H. Qu, H. Fu, Z. Han, and Y. Sun, "Biomaterials for bone tissue engineering scaffolds: A review," (in Eng), *RSC Advances*, vol. 9, no. 45, pp. 26252-26262, 2019.
- [8] D. T. Dixon, and C. T. Gomillion, "Conductive scaffolds for bone tissue engineering: Current state and future outlook," (in Eng), *Journal of Functional Biomaterials*, vol. 13, no. 1, 2021.
- [9] M. Ferraz, F. Monteiro, and C. Manuel, "Hydroxyapatite nanoparticles: A review of preparation methodologies," *Journal of applied biomaterials & biomechanics: Journal of Applied Biology and Biotechnology*, vol. 2, pp. 74-80, 2003.

- [10] M. Eilbagi, R. Emadi, K. Raeissi, M. Kharaziha, and A. Valiani, "Mechanical and cytotoxicity evaluation of nanostructured hydroxyapatite-bredigite scaffolds for bone regeneration," *Materials Science and Engineering: C*, vol. 68, pp. 603-612, 2016.
- [11] K. Aoki, and N. Saito, "Biodegradable polymers as drug delivery systems for bone regeneration," (in Eng), *Pharmaceutics*, vol. 12, no. 2, 2020.
- [12] S. Hassanajili, A. Karami-Pour, A. Oryan, and T. Talaei-Khozani, "Preparation and characterization of PLA/PCL/HA composite scaffolds using indirect 3D printing for bone tissue engineering," *Materials Science and Engineering: C*, vol. 104, p. 109960, 2019.
- [13] F. Donnalaja, E. Jacchetti, M. Soncini, and M. T. Raimondi, "Natural and synthetic polymers for bone scaffolds optimization," (in Eng), *Polymers (Basel)*, vol. 12, no. 4, 2020.
- [14] S. Bhushan, S. Singh, T. K. Maiti, C. Sharma, D. Dutt, S. Sharma, C. H. Li, E. M. T. Eldin, "Scaffold fabrication techniques of biomaterials for bone tissue engineering: A critical review," *Bioengineering*, vol. 9, no. 12, 2022.
- [15] J. Xing, M. Zhang, X. Liu, C. Wang, N. Xu, and D. Xing, "Multi-material electrospinning: from methods to biomedical applications," *Materials Today Bio*, vol. 21, p. 100710, 2023.
- [16] C. Wang, W. Huang, Y. Zhou, L. He, Z. He, Z. Chen, X. He, S. Tian, J. Liao, B. Lu, Y. Wei, and M. Wang, "3D printing of bone tissue engineering scaffolds," *Bioactive Materials*, vol. 5, no. 1, pp. 82-91, 2020.
- [17] H. J. Park, O. J. Lee, M. C. Lee, B. M. Moon, H. W. Ju, J. M. Lee, J-H. Kim, D. W. Kim, and C. Park, "Fabrication of 3D porous silk scaffolds by particulate (salt/sucrose) leaching for bone tissue reconstruction," *International Journal of Biological Macromolecules*, vol. 78, pp. 215-223, 2015.
- [18] D. Mao, Q. Li, D. Li, Y. Tan, and Q. Che, "3D porous poly(ϵ -caprolactone)/58S bioactive glass-sodium alginate/gelatin hybrid scaffolds prepared by a modified melt molding method for bone tissue engineering," *Materials & Design*, vol. 160, pp. 1-8, 2018.
- [19] Y. Nam, J. Yoon, and T. Park, "A novel fabrication method for macroporous scaffolds using gas foaming salt as porogen additive," *Journal of Biomedical Materials Research*, vol. 53, pp. 1-7, 2000.
- [20] J. D. Chen, Y. Wang, and X. Chen, "In situ fabrication of nano-hydroxyapatite in a macroporous chitosan scaffold for tissue engineering," (in Eng), *Journal of Biomaterials Science, Polymer Edition*, vol. 20, no. 11, pp. 1555-65, 2009.
- [21] R. Govindan, F. L. Gu, S. Karthi, and E. K. Girija, "Effect of phosphate glass reinforcement on the mechanical and biological properties of freeze-dried gelatin composite scaffolds for bone tissue engineering applications," *Materials Today Communications*, vol. 22, p. 100765, 2020.
- [22] T. L. Conrad and R. K. Roeder, "Effects of porogen morphology on the architecture, permeability, and mechanical properties of hydroxyapatite whisker reinforced polyetheretherketone scaffolds," *Journal of the Mechanical Behavior of Biomedical Materials*, vol. 106, p. 103730, 2020.
- [23] Y. S. Cho, B.-S. Kim, H.-K. You, and Y.-S. Cho, "A novel technique for scaffold fabrication: SLUP (salt leaching using powder)," *Current Applied Physics*, vol. 14, no.3, pp. 371-377, 2014.
- [24] M. Alizadeh, F. Abbasi, A. B. Khoshfetrat, and H. Ghaleh, "Microstructure and characteristic properties of gelatin/chitosan scaffold prepared by a combined freeze-drying/leaching method," *Materials Science and Engineering: C*, vol. 33, no. 7, pp. 3958-3967, 2013.
- [25] Á. Serrano-Aroca, A. Cano-Vicent, R. S. Serra, M. El-Tanani, A. Aijabali, M. Tambuwale, and Y. K. Mishra, "Scaffolds in the microbial resistant era: Fabrication, materials, properties and tissue engineering applications," *Materials Today Bio*, vol. 16, p. 100412, 2022.
- [26] R. Dorati, C. Colonna, I. Genta, T. Modena, and B. Conti, "Effect of porogen on the physico-chemical properties and degradation performance of PLGA scaffolds," *Polymer Degradation and Stability*, vol. 95, no. 4, pp. 694-701, 2010.
- [27] H. Gheisari, E. Karamian, and M. Abdollahi, "A novel hydroxyapatite –Hardystonite nanocomposite ceramic," *Ceramics International*, vol. 41, pp. 5967-5975, 2015.
- [28] E. F. Morgan, G. U. Unnikrisnan, and A. I. Hussein, "Bone mechanical properties in healthy and diseased states," (in Eng), *Annual Review of Biomedical Engineering*, vol. 20, pp. 119-143, 2018.
- [29] A. Chandrasekaran, S. Suresh, and A. Dakshanamoorth "Synthesis and characterization of nano-hydroxyapatite (n-HAP) using the wet chemical technique," *International Journal of Physical Sciences*, vol. 8, pp. 1639-1645, 2013.
- [30] M. Murugesan, D. Mangalaraj, P. Nagamony, and C. Viswanathan, "Core-shell hydroxyapatite/Mg nanostructures: Surfactant free facile synthesis, characterization and their in vitro cell viability studies against leukaemia cancer cells (K562)," *RSC Advances*, vol. 5, 2015.
- [31] E. Åkerlund, A. Diez-Escudero, A. Grzeszczak, and C. Persson, "The Effect of PCL Addition on 3D-Printable PLA/HA composite filaments for the treatment of bone defects," *Polymers*, vol. 14, no. 16, p. 3305, 2022.
- [32] B. W. Chieng, N. Ibrahim, W. Yunus, and M. Hussein, "Effects of graphene nanoplatelets on poly(lactic acid)/poly (ethylene glycol) polymer nanocomposites," *Polymers*, vol. 6, pp. 93-104, 2013.
- [33] P. Singla, R. Mehta, D. Berek, and S. Upadhyay, "Microwave assisted synthesis of poly(lactic acid) and its characterization using size exclusion chromatography," *Journal of Macromolecular Science Part A Pure and Applied Chemistry*, vol. A49, 2012.
- [34] A. Zimina, F. Senatov, R. Choudhary, E. Kolesnikov, N. Anisimova, M. Kiselevskiy, P. Orlova, N. Strukova, M. Generalova, V. Mansikh, A. Gromov, and A. Karyagina, "Biocompatibility and physico-chemical properties of highly porous PLA/HA scaffolds for bone reconstruction," (in Eng), *Polymers (Basel)*, vol. 12, no. 12, 2020.
- [35] J. Su, J. Teng, Z. Xu, and Y. Li, "Effects of hydroxyapatite content on mechanical properties and in-vitro corrosion behavior of ZK60/HA composites," vol. 111, no. 8, pp. 621-631, 2020.

- [36] S. Ufere, and N. S. P. C. Csci, "Fabrication and characterization of PCL/HA/PPY composite scaffold using freeze-drying technique," *Journal Teknologi*, vol. 78, 2016.
- [37] Z. Cui, W. Li, L. Cheng, D. Gong, W. Cheng, and W. Wang, "Effect of nano-HA content on the mechanical properties, degradation and biocompatible behavior of Mg- Zn/HA composite prepared by spark plasma sintering," *Materials Characterization*, vol. 151, pp. 620-631, 2019.
- [38] T.-T. Li, Y. Zhang, H.-T. Ren, H.-K. Peng, C.-W. Lou, and J.-H. Lin, "Two-step strategy for constructing hierarchical pore structured chitosan–hydroxyapatite composite scaffolds for bone tissue engineering," *Carbohydrate Polymers*, vol. 260, p. 117765, 2021.
- [39] M. V. Chaikina, N. Bulina, O. Vinokurova, K. Gerasimov, I. Y. Prosanov, N. Kompankov, O. Lapina, E. Papulovskiv, A. Ishchenko, and S. Makarova, "Possibilities of mechano-chemical synthesis of apatites with different Ca/P ratios," *Ceramics*, vol. 5, no. 3, pp. 404-422, 2022.
- [40] M. R. B. M. Roslan, N. F. M. Nasir, R. Khalid, N. F. Mohammad, C. E. Meng, N. N. N. Hashim, B. C. You, M. S. A. Majid, and N. A. M. Amin, "The optimization of the hydroxyapatite (HA) material characteristics produced from corbiculacea (Etok) shells," *Journal of Physics: Conference Series*, vol. 1372, p. 012077, 2019.
- [41] S. Best, B. Sim, M. Kayser, and S. Downes, "The dependence of osteoblastic response on variations in the chemical composition and physical properties of hydroxyapatite," *Journal of Materials Science: Materials in Medicine*, vol. 8, no. 2, pp. 97-103, 1997.
- [42] N. Aboudzadeh, A. Khavandi, J. Javadpour, M. A. Shokrgozar, and M. Imani, "Effect of dioxane and N-Methyl-2-pyrrolidone as a solvent on biocompatibility and degradation performance of PLGA/nHA scaffolds," (in Eng), *Iranian Biomedical Journal*, Full Length vol. 25, no. 6, pp. 408-416, 2021.
- [43] M. Haugh, C. Murphy, and F. O'Brien, "Novel freeze-drying methods to produce a range of collagen–glycosaminoglycan scaffolds with tailored mean pore sizes," *Tissue engineering. Part C, Methods*, vol. 16, pp. 887-94, 2009.
- [44] Y. Shafieyan, S. Sharifi, M. Imani, M. Shokrgozar, N. Aboudzadeh, and M. Atai, "A biocompatible compositebased on poly($\hat{1}\mu$ -caprolactonefumarate) and hydroxyapatite," *Polymers for Advanced Technologies*, vol. 22, pp. 2182-2190, 2011.
- [45] G. Huang, L. Xu, J. Wu, S. Wang, and Y. Dong, "Gelatin/ bioactive glass composite scaffold for promoting the migration and odontogenic differentiation of bone marrow mesenchymal stem cells," *Polymer Testing*, vol. 93, p. 106915, 2021.
- [46] R. Radakisnin, M. S. A. Majid, M. R. M. Jamir, M. F. M. Tahir, C. E. Meng, and H. A. Alshahrani, "Physical, thermal, and mechanical properties of highly porous polylactic acid/cellulose nanofibre scaffolds prepared by salt leachingtechnique," *Nanotechnology Reviews*, vol. 10, no. 1, pp. 1469-1483, 2021.
- [47] Z. Shahbazarab, A. Teimouri, A. N. Chermahini, and M. Azadi, "Fabrication and characterization of nanobiocomposite scaffold of zein/chitosan/nanohydroxyapatite prepared by freeze-drying method for bone tissue engineering," *International Journal of Biological Macromolecules*, vol. 108, pp. 1017-1027, 2018.
- [48] P. Kazimierczak, A. Benko, K. Palka, C. Canal, D. Kolodynska, and A. Przekora, "Novel synthesis method combining a foaming agent with freeze-drying to obtain hybrid highly macroporous bone scaffolds," *Journal of Materials Science & Technology*, vol. 43, pp. 52-63, 2020.
- [49] S. Bose, M. Roy, and A. Bandyopadhyay, "Recent advances in bone tissue engineering scaffolds," *Trends in Biotechnology*, vol. 30, no. 10, pp. 546-554, 2012.